THE JOURNAL OF PHYSICAL CHEMISTRY C

ARTICLE

pubs.acs.org/JPCC

Hydration Properties and Interlayer Organization of Water and Ions in Synthetic Na-Smectite with Tetrahedral Layer Charge. Part 2. Toward a Precise Coupling between Molecular Simulations and Diffraction Data

Eric Ferrage,[*,†] Boris A. Sakharov,[‡] Laurent J. Michot,[§] Alfred Delville,[∥] Allan Bauer,[§] Bruno Lanson,[⊥] Sylvain Grangeon,[⊥] Gilles Frapper,[#] Mónica Jiménez-Ruiz,[▼] and Gabriel J. Cuello[▼,○]

[†]Laboratoire Hydrogéologie, Argiles, Sols et Altérations, UMR6269-CNRS, Université de Poitiers, 40 avenue du Recteur Pineau, 86022 Poitiers Cedex, France

[‡]Geological Institute, Russian Academy of Sciences, 7 Pyzhevsky street, 119017 Moscow, Russia

[§]Laboratoire Environnement et Minéralurgie, CNRS-Nancy Université, UMR 7569, BP40 54501, Vandoeuvre Cedex, France

[∥]Centre de Recherche sur la Matière Divisée, CNRS-Université d'Orléans, UMR 6619, 1B rue de la Férollerie, 45071 Orléans Cedex 2, France

[⊥]Mineralogy & Environments, LGCA — Maison des Géosciences, CNRS — Université Joseph Fourier, BP53, 38041 Grenoble Cedex 9, France

[#]Groupe de Chimie Quantique Appliquée, LACCO, UMR 6503-CNRS, Université de Poitiers, 40 avenue du Recteur Pineau, 86022 Poitiers Cedex, France

[▼]Institut Laue-Langevin, BP156, 38042 Grenoble Cedex, France

[○]IKERBASQUE, Basque Foundation for Science, 48011 Bilbao, Spain

ABSTRACT: A specific methodology was developed to collate the interlayer configurations resulting from Grand-Canonical Monte Carlo (GCMC) simulations with experimental X-ray and neutron diffraction data for two synthetic Na-saturated saponites having contrasting layer charge. Numerical simulations were performed assuming different existing sets of atomic partial charge and Lennard-Jones parameters for clay and water. For each parameter set and for the two samples in both the mono- and bihydrated states, the water contents resulting from GCMC simulations were first compared to water vapor desorption gravimetry data. The density distributions of interlayer species were then used to generate 00*l* intensities that were compared to X-ray and neutron diffraction data, the latter being recorded on both hydrogenated and deuterated specimens. The CLAYFF model [Cygan et al. *J. Phys. Chem. B* **2004**, *108*, 1255] is shown to better account for water content and organization compared to the model developed by Skipper et al. (*Clays Clay Miner.* **1995**, *43*, 285) and modified by Smith (*Langmuir* **1998**, *14*, 5959). However, diffraction patterns calculated for bihydrated samples from CLAYFF simulations did not match satisfactorily the diffraction data. Lennard-Jones parameters were thus modified for oxygen atoms from the clay layer. When combined with the SPC/E water model, this modified version of CLAYFF allows matching experimental water contents and fitting the complete set of diffraction data. Relevant information may thus be derived on the influence of layer charge on the orientational properties of interlayer water molecules which differs for the different clay models. Finally, the approach used in the present study proved powerful for assessing atomic interaction parameters considered for computational simulations.

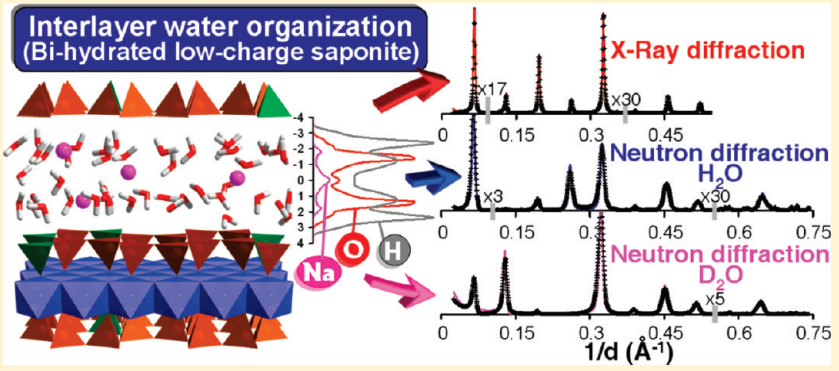

INTRODUCTION

Understanding water—smectite interactions and the structural and dynamical properties of confined water molecules in these mineral structures is of prime importance for many natural processes. Smectites control indeed most of the physical and chemical properties of the numerous environments where they are found, such as soils, sedimentary rocks, engineered barriers for waste confinement, etc.[1−8] For example, the variable hydration

Received: June 4, 2010
Revised: November 12, 2010
Published: January 10, 2011

Table 1. Structure Parameters Used for GCMC Simulations, XRD, and ND 00*l* Reflection Modeling of Saponites Exhibiting Different Hydration States

sample	main hydr. state[a]	salt[b]	target RH[c]	measured RH[d]	layer content 2W/1W/0W[e]	LT 1W[f]	LT 2W[f]	crystalline water content[g]
S−$Na_{0.8}$	1W	$MgCl_2$	33	∼32	2/95/3	12.46	15.01	4.9−6.7
S−$Na_{0.8}$	2W	NaCl	75	∼75	95/3/2	13.10	15.29	10.5−12.8
S−$Na_{1.4}$	1W	LiCl	11	∼16	2/97/1	12.27	14.86	4.9−6.3
S−$Na_{1.4}$	2W	KCl	85	∼85	96/3/1	12.90	15.00	10.9−13.4

[a] Prevalent hydration state in which the interlayer species organization was characterized. [b] Chemicals used to prepare saturated salt solutions for sample equilibration at different relative humidities. [c] Theoretical relative humidities with the salts listed in b.[30] [d] Experimental relative humidities with the salts listed in b (±2% RH). [e] Relative proportion of the different hydration states determined from XRD profile modeling[10] for the RH values given in d. 2W, 1W, and 0W stand for bihydrated, monohydrated, and dehydrated layers, respectively. [f] LT, layer thickness in Å, for 1W and 2W layers. [g] Content of crystalline water (in mmol of H_2O per gram of dry clay) estimated from the combination of water vapor desorption experiments[68] and XRD profile modeling[10] (see text for details).

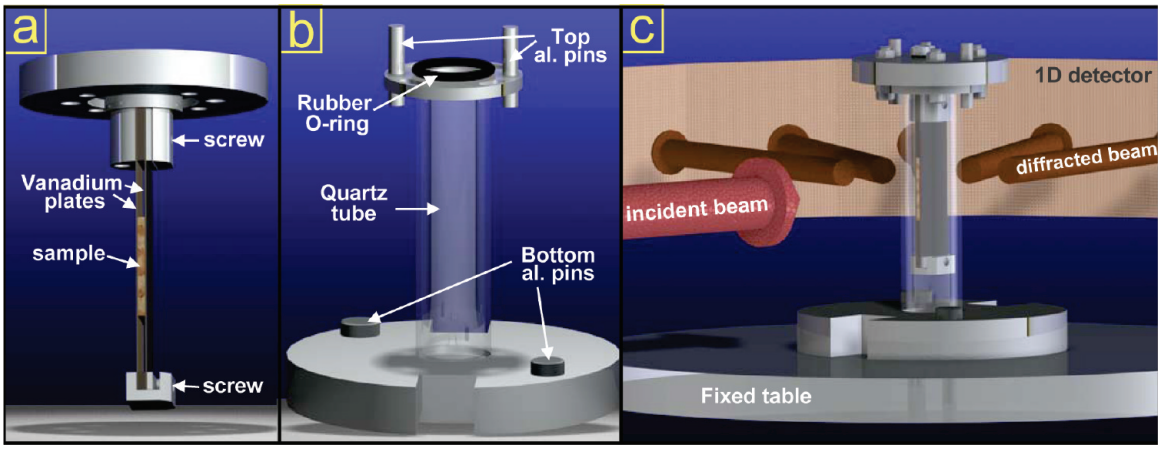

Figure 1. Sample cell designed for neutron diffraction experiments on the D4 instrument of Institut Laue-Langevin (Grenoble, France). (a) The sample is sandwiched between two vanadium plates (2×8 cm^2, 0.5 mm thickness) and inserted into a quartz tube. (b) Top alignment pins were used to maintain identical for all sample cells the orientation between the aluminum hood supporting the sample and the quartz tube. Bottom alignment pins were used to orientate the pedestal of the sample holder with respect to a horizontal plate attached to the instrument for the whole experiment. (c) During experiments, the angle between the incident beam and the sample is thus fixed, and the diffracted intensities are collected by nine 1D-detectors.

and the expansion behavior of smectites can allow the self-healing of bentonite-based engineered barriers and thus the preservation of their low hydraulic conductivity and high sorption capacity, thus impacting the transfer of solutes. In addition to this environmental importance, smectite minerals are appropriate for studying the behavior of two-dimensional confined fluids.[9] In particular, synthetic smectite analogues whose surface chemistry can be accurately controlled represent promising model systems for investigating the structure and dynamics of confined water.

In the first article of the present series,[10] the hydration properties of two synthetic Na-saturated saponites with contrasted layer charge were investigated by modeling X-ray diffraction (XRD) patterns collected along the water vapor desorption isotherm. It was in particular possible to analyze finely the various types of water molecules (crystalline vs pore water) in unsaturated conditions and to determine their distribution balance as a function of relative humidity (RH). The optimized interlayer configuration models remain however rather simple (simplistic?), and questions regarding the differentiation between water molecules coordinated or not to interlayer cations and the role played by the orientation of water molecules on smectite reactivity cannot be answered by such structural studies. Over the last two decades, numerical simulations have thus been developed to provide new perspectives for the characterization of confined fluid structural properties and for the prediction of smectite reactivity evolution upon environmental changes.[11−25] The results of Monte Carlo simulations depend however on the set of partial atomic charge and Lennard-Jones (LJ) parameters used to evaluate Coulombic and van der Waals interactions, respectively. To take full advantage of these two complementary approaches, it is thus crucial to derive consistent models from both numerical simulations and XRD data analysis. A few attempts have been made to generate 00*l* reflection intensities from computed configurations of interlayer species and to match the calculated patterns with diffraction data.[25,26] These studies have consistently shown that the two approaches could be conciliated. However, the increased sensitivity of neutrons, compared to X-rays, for light interlayer species such as (heavy) water undoubtedly makes neutron diffraction a more robust test for the validity of computational results.[25,27−29]

The present study aims at assessing the validity of Monte Carlo simulations performed in the Grand-Canonical ensemble (GCMC) using a dual confrontation. Water contents calculated from GCMC simulations will be collated to those obtained from water vapor desorption gravimetry. In addition, optimized positions of interlayer cations and water molecules will be used to

Table 2. Different Sets of Lennard-Jones Parameters and Partial Atomic Charges Used for GCMC Simulations

species	charge (e)	D_o (kJ mol^{-1})	R_o (Å)
CLAYFF force field[a]			
bridging oxygen	−1.05000	6.5063×10^{-1}	3.5532
bridging oxygen with tetrahedral substitution	−1.16875	6.5063×10^{-1}	3.5532
hydroxyl oxygen	−0.95000	6.5063×10^{-1}	3.5532
tetrahedral aluminum	1.57500	7.7058×10^{-6}	3.7064
tetrahedral silicon	2.10000	7.7058×10^{-6}	3.7064
hydroxide magnesium	1.05000	3.7806×10^{-6}	5.9090
hydroxyl hydrogen	0.42500	0	0
aqueous sodium ion[a]	1.00000	5.4470×10^{-1}	2.6378
Skipper/Smith's force field[b,c]			
tetrahedral oxygen	−0.80000	6.5000×10^{-1}	3.5532
octahedral oxygen	−1.00000	6.5000×10^{-1}	3.5532
hydroxyl oxygen	−1.42400	6.5000×10^{-1}	3.5532
tetrahedral aluminum	0.20000	1.3180×10^{1}	2.0653
tetrahedral silicon	1.20000	1.318×10^{1}	2.0653
hydroxide magnesium	2.00000	0	0
hydroxyl hydrogen	0.42400	0	0
aqueous sodium ion	1.00000	5.4470×10^{-1}	2.6378
water SPC model[d]			
water oxygen	−0.82000	6.5063×10^{-1}	3.5532
water hydrogen	0.41000	0	0
water SPC/E model[e]			
water oxygen	−0.84760	6.5063×10^{-1}	3.5532
water hydrogen	0.42380	0	0

[a] Cygan et al.[59] [b] Skipper et al.[62] [c] Smith.[18] [d] Berendsen et al.[63] [e] Berendsen et al.[64]

calculate X-ray and neutron diffraction (ND) patterns that will be quantitatively fitted to data. Such thorough collation will be performed for two synthetic saponites having different layer charges and hydration states [i.e., the mono- (1W) and bihydrated states (2W)]. Different sets of atomic charge and LJ parameters reported in the literature for clays and water will also be assessed. The above-described collation will be shown to allow the discrimination between different clay and water models and the improvement of existing models to better account for both organizational and orientational properties of interlayer water.

MATERIALS AND METHODS

Sample Preparation for Neutron Diffraction. The synthetic Na-saponites used were those described in the first part of this work.[10] Their structural formula is $Na_x(Si_{8-x},Al_x)(Mg_6)O_{20}(OH)_4$, with x = 0.8 and 1.4, and the two samples are hereafter referred to as S−$Na_{0.8}$ and S−$Na_{1.4}$, respectively. Sample preparation for XRD experiments is described elsewhere.[10] For ND experiments, eight oriented specimens (2×3 cm^2 in the layer plane and 2 mm perpendicularly) were prepared (two samples, each with either H_2O or D_2O and for two RH values). For D_2O specimens, the oriented films were dried at 120 °C before being equilibrated in deuterated $CuSO_4$-saturated solution vapor (RH ∼98%). This procedure was repeated three times to ensure the complete replacement of H_2O. Finally, all specimens were equilibrated for two weeks at the desired RH values starting from nearly saturated conditions (RH∼98%), which is along the desorption isotherm. The RH values used for ND analyses are reported in Table 1. These values were chosen to minimize hydration heterogeneity, that is, to avoid the coexistence of layers having different hydration states,[10] and maintained with saturated salt solutions prepared in parallel in H_2O or D_2O.[30]

Neutron Diffraction and ND Profile Modeling of 00*l* Reflections. Neutron diffraction patterns were recorded on the two-axis D4 diffractometer at the Institut Laue-Langevin in Grenoble, France.[31] The operating wavelength was 0.6966 Å, and the takeoff angle between the tube and the sample was kept constant with an angle value optimizing the high-angle resolution. Intensities were collected on nine 160 mm wide 1D position sensitive detectors, positioned at a distance of 116 cm, giving an angular spacing of 0.125°2θ. Although the setup allows recording intensities over an angular range of 1−138°2θ (40−0.37 Å), 00*l* reflections were never observed above 30°2θ (1.35 Å). Six homemade cells were designed for obtaining diffraction patterns on oriented specimens (2×2 cm^2, 1.0 mm thickness) under controlled conditions (Figure1). Before analysis, samples were kept for about 6 h in the sample cells in which saturated salt solutions prevented any hydration/dehydration during sample mounting and data collection.

Data were corrected for z-shift and detectors efficiency, and 00*l* reflection positions were calibrated using quartz and clay standards. A program similar to that used to reproduce XRD data was used for fitting the experimental ND profiles over the 2−30°2θ angular range. This program relies on the algorithms developed by Sakharov and co-workers,[32−34] and includes the specificity of neutron radiation relative to the Lorentz-Polarization factor calculation. Since the neutron beam was nonpolarized, the polarization function was removed, while the Lorentz (L) contribution was calculated as follows

$$L = 1/[2 \sin(2\theta) \cos(\theta)] \quad (1)$$

The z-coordinates of all atoms building up the 2:1 layer were set as determined for vermiculite minerals.[35] Calculations of ND (and XRD) profiles were performed taking into account the hydration heterogeneities (proportion of 0W, 1W, and 2W layers) reported in Table 1. The interlayer species density profiles calculated from GCMC simulation (see below) were introduced for the dominant layer (Table 1), whereas the interlayer configurations of the other layer types were set as described by Ferrage et al.[10] The coherent scattering domain (CSD) size along the c^*-axis (i.e., direction perpendicular to the clay layers) is characterized by a maximum CSD size, set to 50 layers, and by a variable mean CSD size (N).[36] The latter parameter was refined during ND profile fitting, whereas for XRD profiles the values were determined by Ferrage et al.[10]

Grand-Canonical Monte Carlo Simulations. The amount of confined water and the equilibrium states of interlayer species (water and sodium ions) for a given RH were derived from GCMC simulations[37−39] using a homemade program.[25,40−42] The simulation box was considered rigid and included three clay layers (and interlayers) that extend 6 × 4 unit-cells along the a and b directions, respectively. Each 2:1 layer was shifted by $-a/3$ (layer displacement) with respect to the preceding layer, leading to a face-to-face configuration for ditrigonal cavities from adjacent layers independent of the layer thickness value. The tetrahedral

substitution sites were selected randomly in each clay layer using an exclusion rule; i.e., two aluminum atoms cannot occupy neighboring tetrahedra, in agreement with spectroscopic results obtained on these samples.[43] The Al-for-Si substitutions are fully compensated by interlayer sodium ions. The actual layer charge considered for GCMC simulations was then 0.83 and 1.42 for S−$Na_{0.8}$ and S−$Na_{1.4}$ samples, respectively.

The total electrostatic energy was determined by evaluating the Coulombic and van der Waals terms for each atom−atom interaction in the system. The Coulombic contribution was calculated using the following equation

$$E_{\mathrm{Coul}} = \frac{e^2}{4\pi\varepsilon_0}\sum_{i\neq j}\frac{q_i q_j}{r_{ij}} \quad (2)$$

where the energy of the interaction is inversely proportional to the separation distance r_{ij}. Parameters q_i and q_j correspond to the partial charges of two interacting atoms; e is the charge of the electron (1.60218×10^{-19} C); and ε_0 is the dielectric permittivity of the vacuum (8.85419×10^{-12} C^2/J m). The van der Waals energy term is represented by the conventional Lennard-Jones (LJ) function

$$E_{\mathrm{VDW}} = \sum_{i\neq j} D_{o,ij}\left[\left(\frac{R_{o,ij}}{r_{ij}}\right)^{12} - 2\left(\frac{R_{o,ij}}{r_{ij}}\right)^{6}\right] \quad (3)$$

where $D_{o,ij}$ and $R_{o,ij}$ are empirical parameters for the atomic pair considered. The interaction parameters between atoms are calculated as the arithmetic mean for the distance parameter R_o (eq 4) and as the geometric mean for the energy parameter, D_o (eq 5)

$$R_{o,ij} = \frac{1}{2}(R_{o,i} + R_{o,j}) \quad (4)$$

$$D_{o,ij} = \sqrt{D_{o,i}D_{o,j}} \quad (5)$$

The Coulomb potential used in these molecular simulations is formulated without any assumption concerning the dielectric constant of the system (eq 2). The effective dielectric constant of the simulated system will be induced by the fluctuations of charge locations and water dipoles. By contrast, Ewald summation is necessary to avoid numerical artifacts introduced by the finite size of the simulation cell. For that purpose, the central simulation cell is surrounded by a set of replica. This whole set of replica is finally immersed in a dielectric media, whose dielectric constant (ε_∞) may be selected in some arbitrary manner. The Ewald energy is finally corrected according to that arbitrary choice

$$E_{\mathrm{Ewald}(\varepsilon_\infty)} = E_{\mathrm{Ewald}(\varepsilon_\infty=\infty)} + \frac{2\pi|M|^2}{V(1+2\varepsilon_\infty)} \quad (6)$$

where V is the total volume of the central simulation cell and M its electric moment. While classical approaches either use $\varepsilon_\infty = \infty$ (metallic surrounding) or $\varepsilon_\infty = 1$ (vacuum), it is generally recommended to select the a priori unknown value of the dielectric constant of the simulated system which was considered here as that of bulk water.

Numerous clay models have been proposed to simulate clay−water[12,14,18,22,44−49] and clay−organics[50−57] interactions. Among these various models, some recent ones have proven particularly efficient in reproducing experimental interfacial energies (±10%) and unit-cell parameters (±0.5%) for dioctahedral minerals.[56−58] Still, as far as clay−water interactions are concerned, two different models adaptable to the case of trioctahedral minerals are widely used in the literature (Table 2). The first one is the CLAYFF force field,[59] whereas the second one uses the LJ and partial charge values derived by Smith and co-workers (Table 2)[18,24,60,61] from the empirical models of Skipper and co-workers.[21,22,62] The latter model is hereafter referred to as Skipper/Smith's force field (S/S-FF). We then decided in the present study to test them extensively in spite of their intrinsic inconsistency in atomic charge assignment and consequent limitations in reproducing the crystal structure of clay minerals.[56−58] Similarly, water models are even more numerous, and in the present study, we only considered two of the most popular ones: the simple point charge (SPC)[63] and the "extended" simple point charge (SPC/E)[64] models (Table 2). Additional self-polarization energy correction was used for the SPC/E model to account for the polarization of condensed-phase water.[64,65]

The GCMC simulations were constituted of 3000 blocks, each with 10 000 elementary steps. For each step, one of the clay interlayers was selected randomly, and with an equal probability an attempt was done to (i) remove a water molecule, (ii) add a water molecule in a random configuration, or (iii) move a randomly chosen cation or water molecule. The atomic positions of saponite layers were fixed during simulations. The 3×10^7 steps allowed stabilizing the number of confined water molecules. During calculations, an Ewald summation[66] was used in addition to the three-dimensional minimum image convention to ensure the convergence of the electrostatic energy. 2196 replicas were used for the summation in the reciprocal space, and a damping parameter was set to 0.19 $Å^{-1}$, leading to an accuracy of better than 0.002.[67] A final run of 200 blocks was performed to generate the equilibrium properties of interlayer species used to generate X-ray and neutron diffraction 00*l* reflections. The water (oxygen and hydrogen) and sodium atomic positions were thus averaged over the three layers and symmetrized relative to the interlayer midplane. The atomic content profiles were generated by subdividing the interlayer distance in 40 slices along the unit-cell c^*-axis.

RESULTS

Methodology. As the main objective of the present study was to combine/couple/cross-validate numerical GCMC simulations and XRD and ND data, a specific methodology was adopted. For each RH value, the layer thickness of the dominant layer (1W or 2W) was determined from XRD data[10] (Table 1) and used to constrain the GCMC simulations with the different water and clay model force fields (Table 2). The water amount then obtained from GCMC simulation for a given RH was added to the water content in the minor layer type (from Tables 1 and 2 of Ferrage et al.[10] for sample S−$Na_{0.8}$ and S−$Na_{1.4}$, respectively), and the total was compared to indicative crystalline water contents reported in Table 1. The range allowed for these latter values was estimated differently for 1W and 2W samples. For 1W saponites, the lower limit was set to a value 10% lower than that determined from water vapor desorption gravimetry experiments, whereas the upper limit was set to a value 10% higher than that determined from XRD profile modeling.[10] Indeed, water vapor desorption gravimetry experiments tend to underestimate the water content of the studied saponites due to the presence of residual water molecules after sample pretreatment.[10,68] For 2W saponites, water amounts derived from water vapor desorption gravimetry experiments can overestimate strongly the content of crystalline

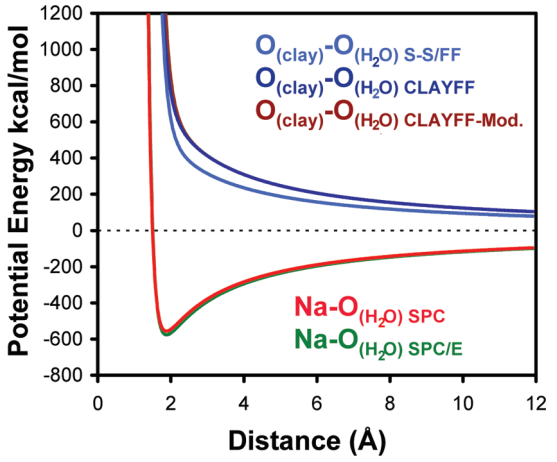

Figure 2. Potential energy curves between water oxygen (SPC/E model) and tetrahedral clay oxygen calculated for the Skipper/Smith's force field (S/S-FF), the CLAYFF clay model, or its modified version (CLAYFF-Mod., see text for details). The influence of SPC and SPC/E water models is shown on the potential energies calculated between interlayer sodium and water oxygen.

water owing to the presence of pore water, and the water content was allowed to vary by ±10% about the XRD-determined value (Table 1).[10] The interlayer water and cation profiles determined from GCMC simulations were introduced next as initial parameters for generating 00*l* reflections either for XRD or ND, for both H_2O and D_2O specimens. The fit quality obtained for these diffraction patterns was used to assess the different models used for GCMC simulations.

Comparison between Existing Force Fields. GCMC simulations depend strongly on the LJ and charge parameters used to calculate electrostatic interactions. When comparing the two force fields used in the present study, the main differences concern the partial charges assigned to cations and anions. Compared to the S/S-FF model, the negative charge of oxygen atoms is delocalized toward O atoms of the 2:1 clay surface in the CLAYFF model (increased from −0.8 e in S/S-FF to −1.05 e in the CLAYFF model, Table 2). This difference modifies the evaluation of the potential energy (Figure 2) and in particular increases the repulsion between O(clay) and O(H_2O) when using the CLAYFF model compared to the S/S-FF model. The charge difference between Si and Al also differs between the two models. The charge difference between Si and Al corresponds to that of the fully charged ions (1.00 e, Table 2) in the S/S-FF clay model with no additional undersaturation of surface oxygen atoms. In the CLAYFF model, this difference is reduced (0.53e, Table 2), and the additional negative charge is supported by the oxygen atoms of the 2:1 layer surface (from −1.05 to −1.17e, Table 2), thus increasing the repulsion between O(clay) and O(H_2O) (Figure 2). The difference between the SPC and SPC/E water models (Table 2) is extremely marginal. The polarization of water molecules is increased for the SPC/E model, whereas the potential energy of the Na−O(H_2O) pair of atoms interaction is almost unaffected (Figure 2).

Sensitivity of the Different Diffraction Methods. X-ray and neutron diffraction have different sensitivity toward atomic species as X-rays interact with electrons whereas neutrons interact with atom cores. This contrast is illustrated in Figure 3 where the relative contributions of the different atomic contributions to the diffracted intensity are shown for a 2W smectite. As expected,

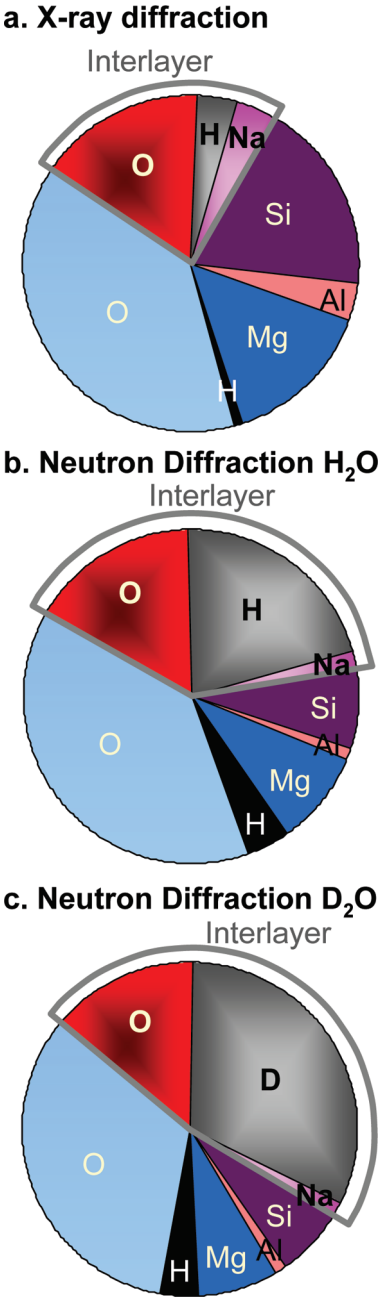

Figure 3. Relative contributions of the different atoms to the structure factor for the three diffraction methods used in the present study. Calculations performed for a bihydrated S−$Na_{1.4}$ with 10 H_2O molecules per $O_{20}(OH)_4$. (a) X-rays for neutral atoms and with atomic scattering factors considered at $\theta = 0$. (b) Neutrons on hydrogenated samples. The absolute value of the scattering length was considered for H atoms. (c) Neutrons on deuterated samples.

XRD is almost insensitive to hydrogen atoms either from water molecules or from the 2:1 layer (Figure 3a). The various atomic contributions are strikingly different for ND (Figure 3b) and can be even modified further by using heavy water (Figure 3c) owing to the respective coherent scattering length of H and D atoms (−3.739 and 6.671 fm, respectively). As a result, the contribution to the diffracted intensities of interlayer species increases from ~25% for XRD to ~40% (using H_2O) and ~47% (using D_2O) for neutron diffraction. The contribution of total oxygen

dx.doi.org/10.1021/jp105128r |*J. Phys. Chem. C* 2011, 115, 1867–1881

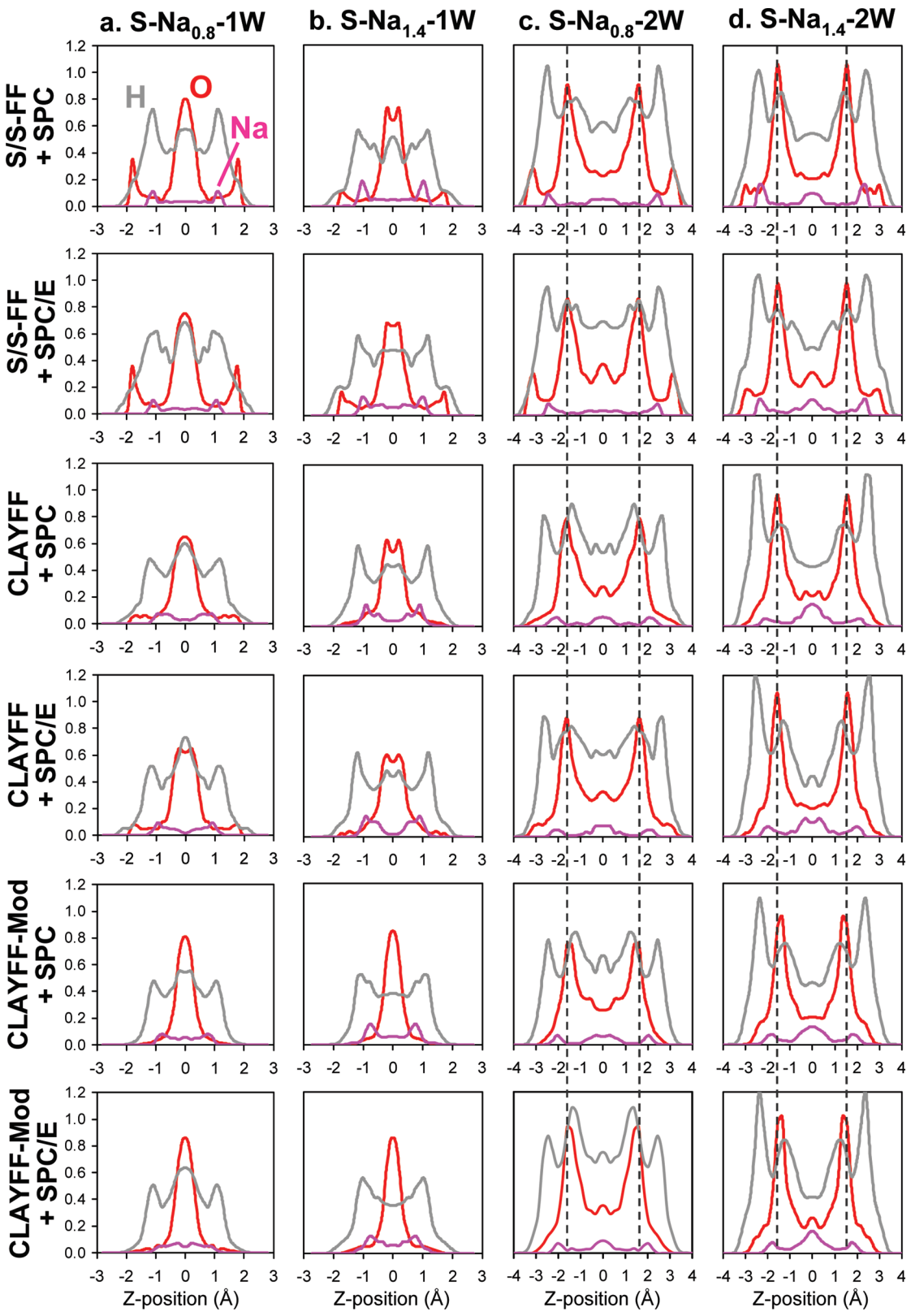

Figure 4. Atomic density profiles (arbitrary units) of oxygen, hydrogen, and sodium atoms generated from GCMC simulations using different force fields to describe the 2:1 clay layer and water molecules. (a) Monohydrated S−$Na_{0.8}$, (b) monohydrated S−$Na_{1.4}$, (c) bihydrated S−$Na_{0.8}$, and (d) bihydrated S−$Na_{1.4}$. Profiles for oxygen, hydrogen, and sodium atoms are shown in red, gray, and pink, respectively. Atomic *z*-coordinates are given in Angströms relative to the interlayer midplane. Lennard-Jones parameters and partial atomic charges are reported in Table 2 for the Skipper/Smith's (S/S-FF) and CLAYFF models, together with parameters of the SPC and SPC/E water models. The parameters relative to the modified CLAYFF model (CLAYFF-Mod.) are listed in Table 4. For bihydrated samples, the vertical dashed lines highlight the influence of the chosen force fields on the positions of oxygen maxima.

dx.doi.org/10.1021/jp105128r |*J. Phys. Chem. C* 2011, 115, 1867–1881

Table 3. Water Contents and Mean Coherent Scattering Domain Sizes Used to Calculate XRD and ND 00*l* Intensities for the Different Clay and Water Models Considered for GCMC Simulations (Tables 2 and 4)

models[a]	N (XRD)[b]	N (ND−H_2O)[b]	N (ND−D_2O)[b]	$n H_2O$ GCMC[c]	total water content[d]
S−$Na_{0.8}$−1W					
S/S-FF + SPC water	15.0	5.0	6.0	6.12	7.66
S/S-FF + SPC/E water	15.0	5.0	6.0	6.43	8.04
CLAYFF + SPC water	15.0	5.0	6.0	4.98	6.27
CLAYFF + SPC/E water	15.0	5.0	6.0	5.37	6.74
CLAYFF-Mod. + SPC water	15.0	5.0	6.0	4.27	5.40
CLAYFF-Mod. + SPC/E water	15.0	5.0	6.0	4.82	6.07
S−$Na_{0.8}$−2W					
S/S-FF + SPC water	12.0	6.0	6.0	10.73	13.36
S/S-FF + SPC/E water	12.0	6.0	6.0	11.06	13.76
CLAYFF + SPC water	12.0	6.0	6.0	9.40	11.73
CLAYFF + SPC/E water	12.0	6.0	6.0	10.18	12.69
CLAYFF-Mod. + SPC water	12.0	6.0	6.0	8.88	11.09
CLAYFF-Mod. + SPC/E water	12.0	6.0	6.0	9.54	11.80
S−$Na_{1.4}$−1W					
S/S-FF + SPC water	14.5	7.0	6.0	5.25	6.47
S/S-FF + SPC/E water	14.5	7.0	6.0	5.75	7.07
CLAYFF + SPC water	14.5	7.0	6.0	4.79	5.91
CLAYFF + SPC/E water	14.5	7.0	6.0	5.04	6.21
CLAYFF-Mod. + SPC water	14.5	7.0	6.0	4.36	5.39
CLAYFF-Mod. + SPC/E water	14.5	7.0	6.0	4.59	5.60
S−$Na_{1.4}$−2W					
S/S-FF + SPC water	16.0	6.0	6.0	10.45	12.80
S/S-FF + SPC/E water	16.0	6.0	6.0	10.87	13.31
CLAYFF + SPC water	16.0	6.0	6.0	10.09	12.37
CLAYFF + SPC/E water	16.0	6.0	6.0	10.28	12.59
CLAYFF-Mod. + SPC water	16.0	6.0	6.0	9.54	11.70
CLAYFF-Mod. + SPC/E water	16.0	6.0	6.0	9.83	12.07

[a] Clay and water models used in GCMC simulations for the dominant mono- (1W) and bihydrated (2W) layers of S−$Na_{0.8}$ and S−$Na_{1.4}$. S−S/FF and CLAYFF-Mod. stand, respectively, for the Skipper/Smith force field and for the version of CLAYFF model modified in the present study. [b] Mean size of the coherent scattering domains along the c^*-axis (N, in layers) for X-ray diffraction (XRD) and neutron diffraction on both hydrogenated and deuterated samples (ND−H_2O and ND−D_2O, respectively). N values for XRD profiles are taken from Ferrage et al.[10] [c] Number of H_2O molecules in the dominant hydrated layer (per $O_{20}(OH)_4$) as computed for the different clay and water models. [d] Total interlayer water content (in mmol of H_2O per gram of dry clay) determined as the sum of interlayer water from all hydrated layers (proportion and water content of minor hydrated layers are given in Table 1).

and sodium atoms remains about constant for all techniques. For these latter cations, their limited contribution to the diffracted intensity indicates that the different techniques are almost insensitive to their position. Note in addition that this description takes into account the contribution of individual atoms considering absolute values for coherent scattering lengths, whereas coherent scattering lengths of oxygen and hydrogen have opposite signs.

Collation between GCMC Simulation Results and Diffraction Data. The distributions of interlayer species derived from GCMC simulations for the different clay and water models are shown in Figure 4. The number of layers in the CSDs and that of water molecules derived from numerical simulations are reported in Table 3. The computed total amounts of crystalline water are compared to the gravimetric data in Figure 5. For all interlayer models considered, calculated 00*l* reflection profiles for XRD and ND on both hydrogenated and deuterated specimen are compared to diffraction data in Figures 6 and 7 for monohydrated S−$Na_{0.8}$ (S−$Na_{0.8}$−1W) and S−$Na_{1.4}$ (S−$Na_{1.4}$−1W), respectively, and in Figures 8 and 9 for bihydrated S−$Na_{0.8}$ (S−$Na_{0.8}$−2W) and S−$Na_{1.4}$ (S−$Na_{1.4}$−2W), respectively.

Simulations of Diffraction Data Using the S/S-FF Model. With this clay model, and independent of the water model used, the water contents obtained for S−$Na_{0.8}$−1W and S−$Na_{1.4}$−1W exceed the upper limit of the possible range (Tables 1 and 3, Figure 5). In addition, when generating 00*l* reflections on the basis of computed interlayer species density profiles (Figure 4), significant misfits are observed with the data (Figures 6a and b and 7a and b), especially when using the SPC/E water model. Misfits are especially severe for the 002 reflection in the XRD patterns of S−$Na_{0.8}$−1W and for the 001, 002, 006, and 008 reflections in the ND−D_2O patterns of both S−$Na_{0.8}$−1W and S−$Na_{1.4}$−1W, whereas ND−H_2O patterns are satisfactorily reproduced. For 2W samples, most of the computed water amounts are in the range of expected contents (Tables 1 and 3, Figure 5), but significant misfits are observed between experimental

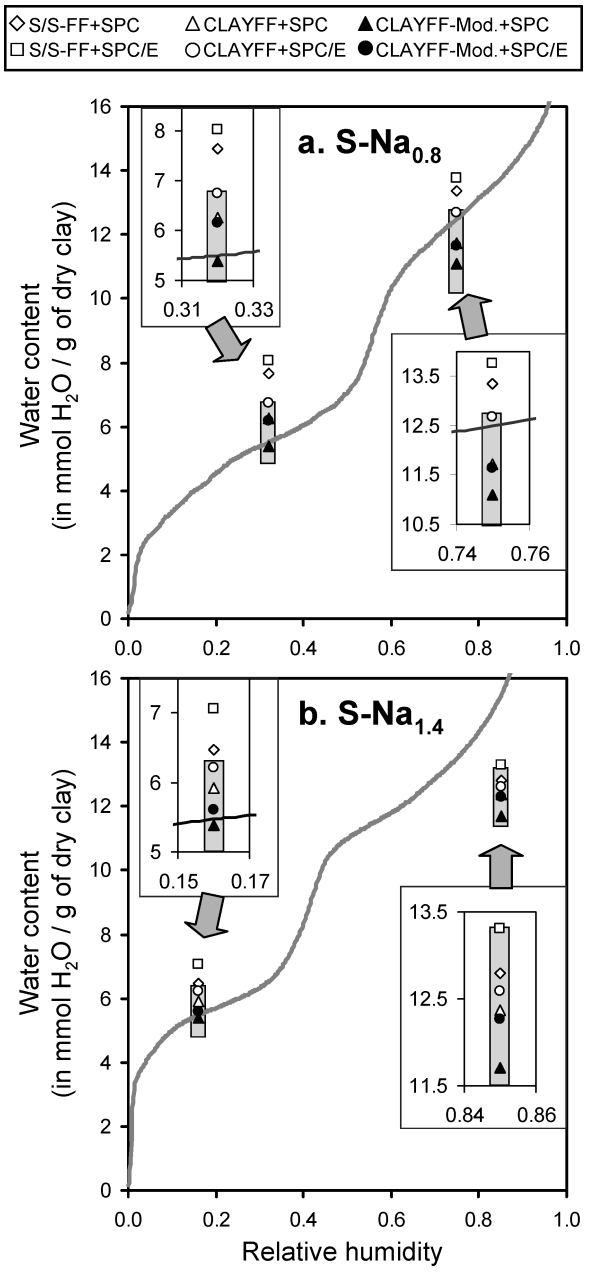

Figure 5. Water contents determined from water vapor desorption isotherms (gray solid line)[68] and derived from GCMC simulations for (a) S−$Na_{0.8}$ and (b) S−$Na_{1.4}$. For mono- and bihydrated states, the gray bars outline the expected contents reported in Table 1. Lennard-Jones parameters and partial atomic charges are reported in Table 2 for the Skipper/Smith's (S/S-FF) and CLAYFF models, together with parameters of the SPC and SPC/E water models. The parameters relative to the modified CLAYFF model (CLAYFF-Mod.) are listed in Table 4.

and calculated diffraction profiles, especially when using the SPC/E water model (Figures 8a and b and 9a and b). For XRD, misfits are especially severe for the 002 and 003 reflections of both samples and for the 004 reflection of S−$Na_{1.4}$−2W. For ND−D_2O patterns, 001, 002, 007, and 0010 reflections are not satisfactorily reproduced for both S−$Na_{0.8}$−2W and S−$Na_{1.4}$−2W, and additional misfits affect the 003 reflection of S−$Na_{1.4}$ and the 006 and 008 reflections of S−$Na_{0.8}$ (Figures 8a and b and 9a and b). As for 1W samples, ND−H_2O data are satisfactorily reproduced except for the 004 reflection of S−$Na_{1.4}$−2W (Figure 9a and b).

Simulations of Diffraction Data Using the CLAYFF Force Field. For both hydration states, the computed water contents fall within the expected range (Tables 1 and 3, Figure 5), the values being systematically higher with the SPC/E model compared to the SPC model. For 1W states, fits of 00*l* reflections are significantly improved compared to the S/S-FF model (Figures 6c and d and 7c and d); calculated XRD and ND−H_2O profiles are in good agreement with the data. For ND−D_2O profiles, improvements are especially noticeable over the low-angle region, the extinction of the 001 reflection being much better reproduced (Figures 6c and d and 7c and d). Some discrepancies remain however visible for the 002, 006, and 008 reflections of the two samples (Figures 6c and d and 7c and d). For 2W states, important misfits remain, especially when using the SPC/E water model, despite significant improvements compared to the S/S-FF model (Figures 8c and d and 9c and d). For example, XRD intensities computed for the 002 and 003 reflections remain lower than the data. For ND−D_2O profiles, the 007 and 0010 reflections are too intense compared to the data for both samples, and the 001/002 and 002/003 intensity ratios are poorly reproduced for S−$Na_{0.8}$−2W and for S−$Na_{0.8}$−2W, respectively (Figures 8c and d and 9c and d).

DISCUSSION

Influence of the Different Clay and Water Force Fields on Interlayer Species Organization. Relevance and Limitations of Existing Clay Force Fields. The different clay and water models considered in GCMC simulations all provide consistent density profiles of interlayer species (Figure 4). Oxygen atoms from H_2O molecules are mainly localized in the interlayer midplane of 1W smectites, whereas hydrogen atoms are partially oriented toward the 2:1 clay layer. Sodium atoms are scattered along the c^*-axis with the presence of higher density planes close to the clay layer, especially for S−$Na_{1.4}$ (Figure 4). In 2W structures, the distribution of interlayer cations presents an additional equilibrium position at the interlayer midplane, and H_2O molecules are localized on both sides of this plane. Despite this global similarity, the calculation of diffraction patterns allows unravelling subtle differences between the interlayer configurations calculated for the different clay and water force fields. For all samples, and independent of the water model used, the interlayer species distributions obtained using the S/S-FF clay model (Figure 4) lead to severe misfits between calculated diffraction profiles and the data (Figures 6, 7, 8, and 9). This model also leads to a systematic overestimation of the amounts of interlayer water, compared to the data (Figure 5). This increased water content is related to the presence of additional water sheets close to the clay surface (Figure 4), induced by the partial charge of oxygen atoms from the clay surface (−0.8 e) which incorrectly accounts for the Coulombic repulsion between clay surfaces and water molecules. Using the CLAYFF model, the negative charge is higher for clay layer oxygen atoms, thus increasing the repulsion between H_2O molecules and the clay layer (Figure 2). In turn, the increased repulsion prevents the presence of H_2O molecules close to the clay layer surface (Figure 4). As a result, the water content is reduced in both 1W and 2W smectites compared to the S/S-FF model and consistent with the experimental values (Figure 5). Although rational, the present interpretation could be

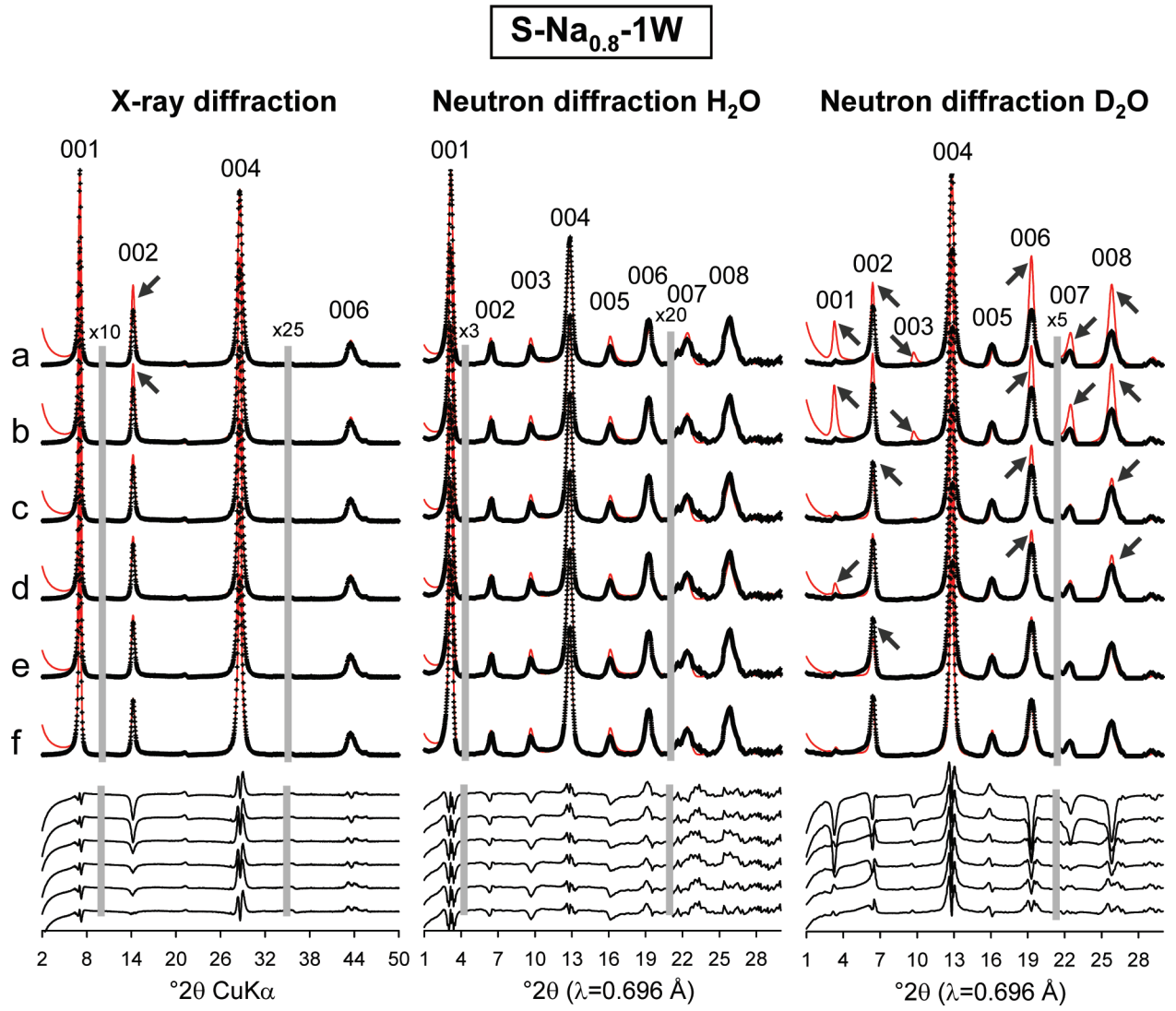

Figure 6. Experimental (black crosses) and calculated (red lines) intensities of 00*l* reflections for monohydrated S−$Na_{0.8}$ and different density profiles of interlayer species. Density profiles were calculated using different clay and water force-fields: (a) S/S-FF+SPC, (b) S/S-FF+SPC/E, (c) CLAYFF+SPC, (d) CLAYFF+SPC/E, (e) CLAYFF-Mod.+SPC, (f) CLAYFF-Mod.+SPC/E (Tables 2 and 4, Figure 4). Difference plots are shown at the bottom of the figure. The vertical gray bars indicate a modified scale factor for the high-angle regions as compared to the low-angle part of the patterns. Solid arrows indicate a significant misfit between experimental and calculated patterns. 00*l* reflections are indexed on the top part of the figure.

complemented by taking into account the contribution of hydrogen atoms when assessing the total potential energy curves.

Modification of the CLAYFF Force Field. Despite the overall improvement of fit quality when using the CLAYFF model, especially for monohydrated structures (Figures 6 and 7), important misfits are still observed between calculated and experimental X-ray and neutron diffraction patterns for 2W smectites. The LJ parameters of atoms within the clay layer and interlayer (sodium) were thus modified in the CLAYFF model to improve the fit of diffraction patterns obtained for 2W smectites. The modifications were performed one at a time, and the impact of the modification was systematically assessed for all diffraction profiles and hydration states. All modifications of the LJ parameters proved unsuccessful for interlayer sodium. Increasing the distance parameter R_o improved the fit quality for S−$Na_{1.4}$−1W (data not shown) and allowed us to decrease the water content. However, this modification did allow a significant improvement of fit quality only for S−$Na_{1.4}$−1W, most likely because of the increased influence of sodium in this sample on water. The most efficient modification of the CLAYFF model was to define independent LJ parameters for oxygen atoms from H_2O molecules and from the clay layer. For oxygen atoms from the clay layer, the distance parameter R_o was increased from 3.553 to 3.800 Å (∼+7%, Table 4) allowing calculated XRD and ND patterns to match closely the data (Figures 6, 7, 8, and 9). The proposed modification, hereafter referred to as the CLAYFF-Mod. model, has a key effect on the position of the oxygen atoms from water molecules (2W state, Figures 4c and d). Increasing the R_o value enhances in turn the repulsion between H_2O molecules and the clay layer, and the equilibrium position of interlayer oxygen atoms is systematically shifted by about 0.15 Å along the c^*-axis toward the interlayer midplane (Figures 4c and d). The resulting shorter distance between the H_2O molecule maximum density and the interlayer midplane strongly affects the XRD relative intensities of the 002 and 003 reflections,[26] allowing for a better fit of the diffraction data recorded on 2W samples. In

dx.doi.org/10.1021/jp105128r |*J. Phys. Chem. C* 2011, 115, 1867–1881

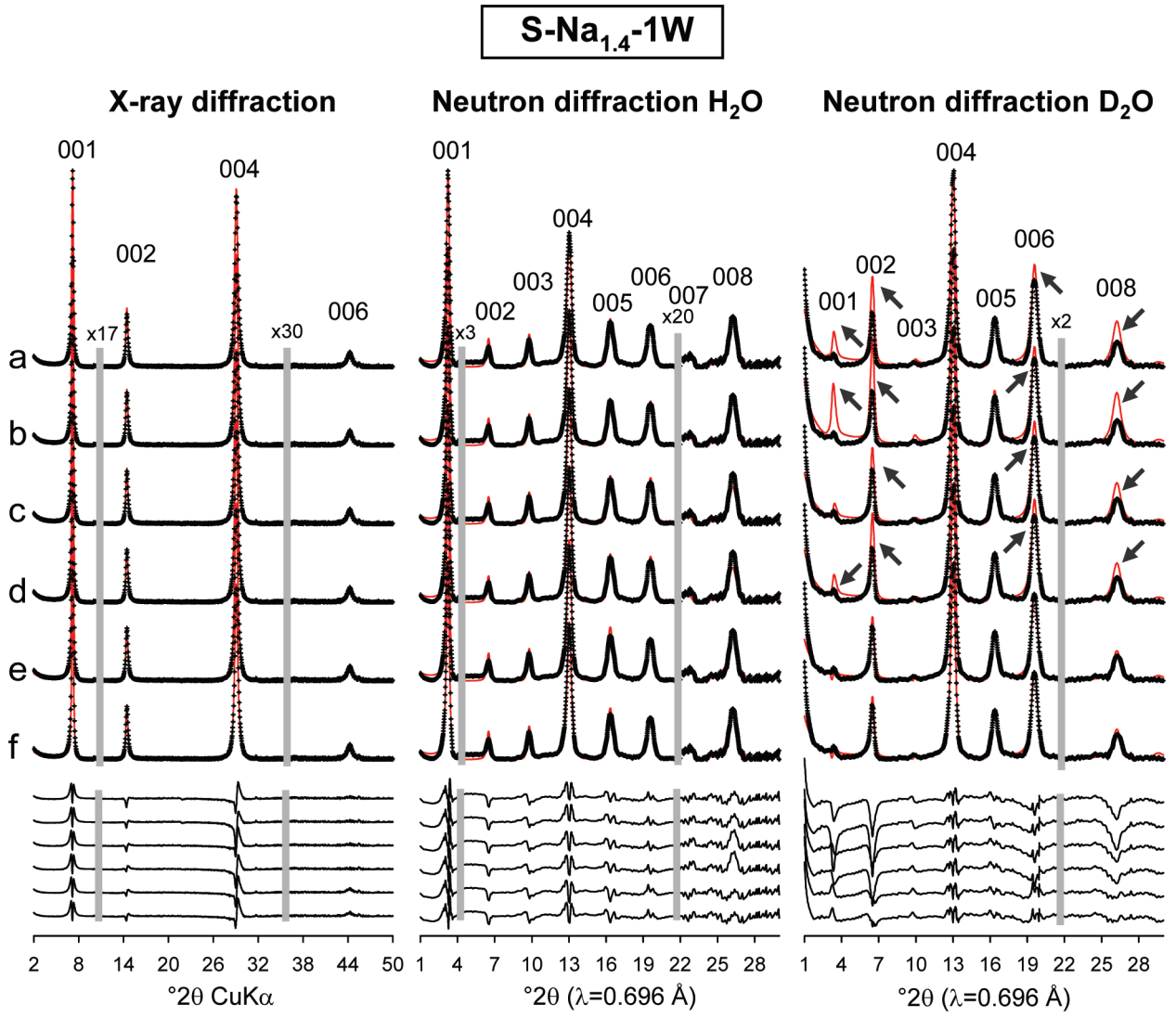

Figure 7. Experimental (black crosses) and calculated (red lines) intensities of 00*l* reflections for monohydrated S−$Na_{1.4}$ and different density profiles of interlayer species. Symbols and notations as in Figure 6.

addition, the increased repulsion between the clay layer and interlayer H_2O decreases the water contents for all samples, but these contents still remain in the expected range (Tables 1 and 3, Figure 5).

Comparison between SPC and SPC/E Water Models. For all clay models considered, the calculated water contents are higher with the SPC/E model than with the SPC model (Figure 5). The difference (~0.5 mmol of H_2O per gram of dried clay) is most likely related to the increased polarizability of H_2O molecules in the SPC/E model and to the induced increased ordering of interlayer H_2O molecules (Figure 4). Oxygen atom distributions are indeed narrower and denser when using the SPC/E model compared to the SPC model (Figure 4). Although the differences may appear marginal, ND−D_2O profiles calculated with the SPC/E model systematically fit the data better. When using the CLAYFF-Mod. model (Table 4) with the SPC model, discrepancies are visible on ND−D_2O profiles: (i) the 002 reflection for S−$Na_{0.8}$−1W (Figure 6), (ii) the 001, 003, 004, and 007 reflections for S−$Na_{0.8}$−2W (Figure 8), and (iii) the 001 and 007 reflections for S−$Na_{1.4}$−2W (Figure 9). These discrepancies are concealed when using the SPC/E water model, thus suggesting that the latter model provides a better description of the organizational properties of interlayer H_2O molecules. This conclusion should however be assessed further. On the other hand, the SPC/E water model leads to water contents that are slightly higher than the gravimetric data for 1W layers (Figure 5). The observed discrepancy is consistent with the hypothesized underestimation of water content determined by gravimetry experiments.[68] The origin of this discrepancy will be discussed further below, together with the ability of the calculated water content to assess the relevance of LJ and partial charge parameters.

Impact of the Adopted Potentials on the Organizational Properties of Interlayer Species. Figure 10 displays interlayer configuration snapshots obtained using CLAYFF-Mod. and SPC/E models. For S−$Na_{0.8}$−1W, H_2O molecules tend to lay parallel to the layer plane or with only one of the hydrogen atoms pointing toward an adjacent clay layer (Figure 10a). In contrast, for S−$Na_{1.4}$−1W (Figure 10b), all H_2O molecules are strongly polarized with their two hydrogen atoms pointing toward adjacent clay layers (Figures 4a and b), most likely to minimize the repulsion between hydrogen and interlayer cations. For the two 2W samples, hydrogen planes are located on both

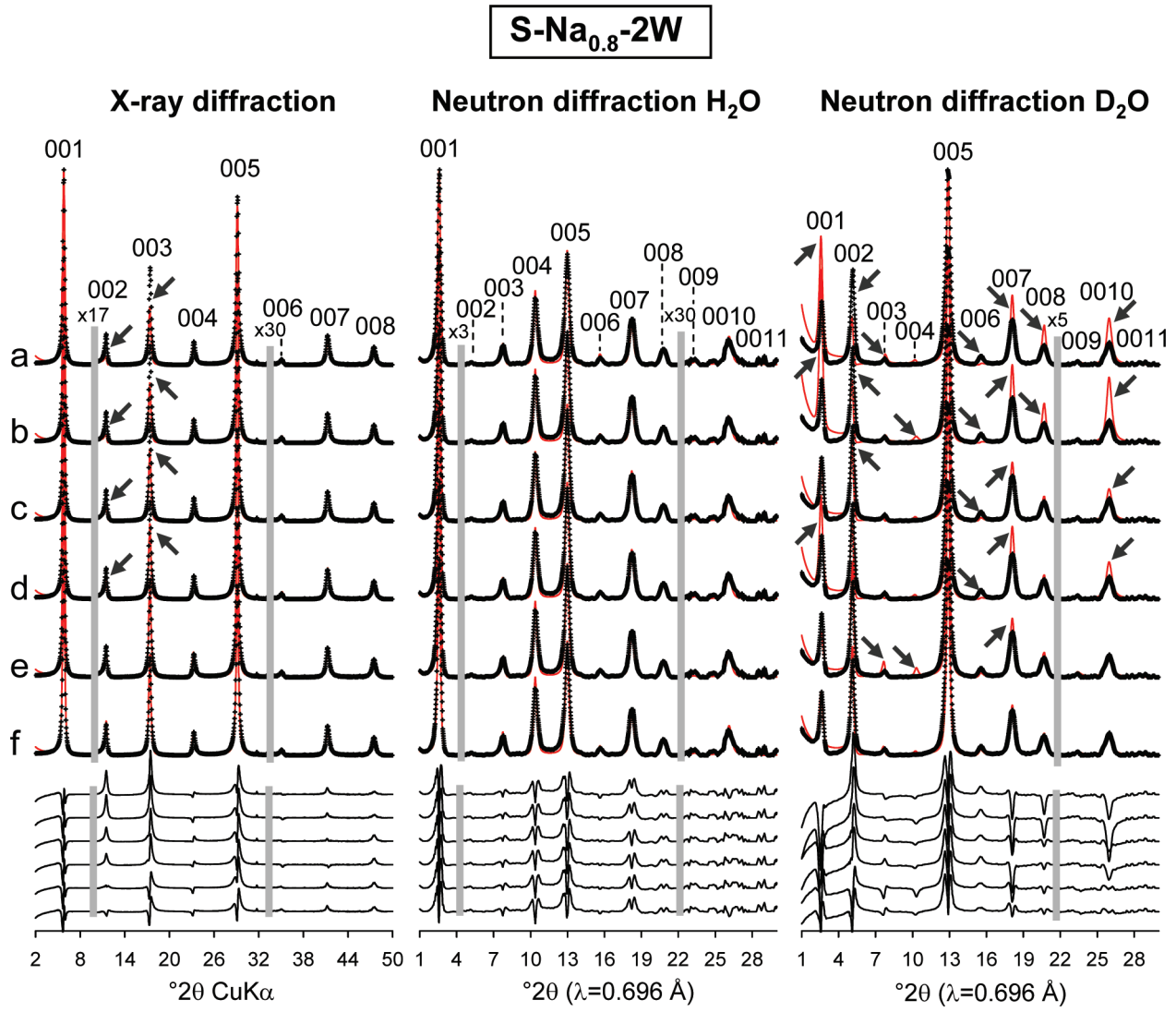

Figure 8. Experimental (black crosses) and calculated (red lines) intensities of 00*l* reflections for bihydrated S−$Na_{0.8}$ and different density profiles of interlayer species. Symbols and notations as in Figure 6.

sides of the oxygen planes, but the high-charge smectites display an increased density for the hydrogen plane located close to the clay surface (Figures 4c and d). As for the 1W state, the increased density of interlayer cations in the latter sample probably contributes, owing to the electrostatic repulsion, to the shift of hydrogen atoms toward the clay surface (Figure 10). Finally, it must be pointed out that this specific orientation of water molecules with layer charge strongly depends on the clay force field model considered. When the using S−S/FF model, the obtained hydrogen density profiles are indeed rather similar for all samples (Figure 4). Such contrasted orientational properties of water with the clay model may in turn impact the dynamical properties of interlayer water molecules which would deserve further investigation. Similarly, owing to their limited proportion and contribution to the diffracted intensity (Figure 3), the full assessment of interlayer cations organization proposed here would deserve further experimental validation.

Experimental Validation of Different Force Field Models. The tight collation between experimental and computational data reported in the present study allowed validating and proposing modifications of the LJ parameters and atomic partial charges used to describe the water−clay interaction. The following sections will discuss the impact of the sample set and of the experimental techniques on the reliability of the approach.

Relevance of the Sample Set. The samples used in the present series of articles are synthetic saponites, with well-controlled and homogeneous chemistry, notably in terms of layer charge. Sample homogeneity is essential as numerical simulations are performed on a very limited clay volume, thus prohibiting de facto sample heterogeneity (e.g., layer charge difference within a layer or from one layer to the other). The present sample homogeneity, and the resulting marginal hydration heterogeneity,[10] thus allows a direct and careful collation of experimental and computational results. In addition, the layer charge difference between two samples adds severe constraints on atomic interaction potentials, as exemplified by the limited influence of sodium LJ potentials on diffraction patterns calculated for Na−$S_{0.8}$−1W, whereas this parameter allowed a close match of experimental and calculated diffraction patterns for Na−$S_{1.4}$−1W. Similarly, examining samples under two hydration states allows assessing almost independently the parameters describing the atomic interactions between the clay layer and the

dx.doi.org/10.1021/jp105128r |*J. Phys. Chem. C* 2011, 115, 1867–1881

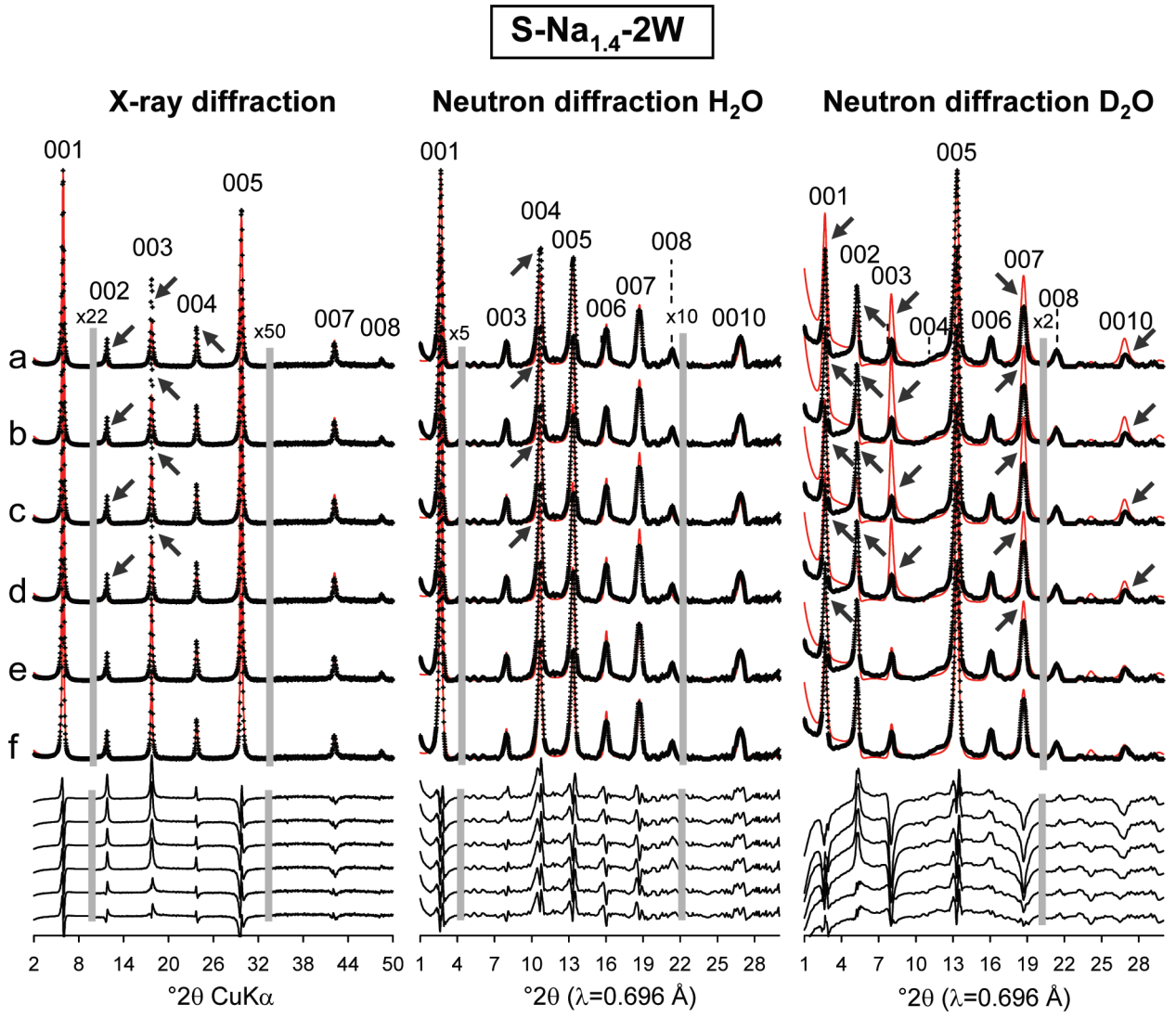

Figure 9. Experimental (black crosses) and calculated (red lines) intensities of 00*l* reflections for bihydrated S−$Na_{1.4}$ and different density profiles of interlayer species. Symbols and notations as in Figure 6.

interlayer cation on the one hand and interlayer H_2O molecules on the other hand.

Interlayer Water Contents. A proper estimate of the number of interlayer water molecules is often considered as a key assessment for GCMC simulations. Consistently, when calculated diffraction profiles fit better the data, water amounts determined from GCMC simulations systematically match more closely those obtained experimentally. However, a careful comparison between experimental and calculated water amounts should take into account that it is nearly impossible to achieve a complete dehydration of the sample before measuring sorption gravimetry isotherms. The residual water content after smectites outgassing is estimated to ~0.5 H_2O molecules per cation and leads to an underestimation of the overall water content.[10,68] The related uncertainty does not allow using small differences in water contents for discriminating between models. In the present work, water content did not allow discriminating CLAYFF and CLAYFF-Mod. models or SPC and SPC/E water models for 1W saponites. In addition, GCMC calculations include only interlayer H_2O molecules (crystalline water), whereas gravimetry experiments probe also water molecules on the external smectite surfaces or in meso- and macropores. At high RH values (2W saponites), it is thus impossible to reconcile experimental and theoretical water contents. Structural considerations should thus complement this

Table 4. Optimized Lennard-Jones Parameters and Partial Atomic Charges Used to Describe the Organization of Interlayer Water (Modified CLAYFF Model, See Text for Details)

species	charge (e)	D_o (kJ mol^{-1})	R_o (Å)
CLAYFF-Mod. force field			
bridging oxygen	−1.05000	6.5063×10^{-1}	3.8000
bridging oxygen with tetrahedral substitution	−1.16875	6.5063×10^{-1}	3.8000
hydroxyl oxygen	−0.95000	6.5063×10^{-1}	3.8000
tetrahedral aluminum	1.57500	7.7058×10^{-6}	3.7064
tetrahedral silicon	2.10000	7.7058×10^{-6}	3.7064
hydroxyde magnesium	1.05000	3.7806×10^{-6}	5.9090
hydroxyl hydrogen	0.42500	0	0
aqueous sodium ion	1.00000	5.4470×10^{-1}	2.6378

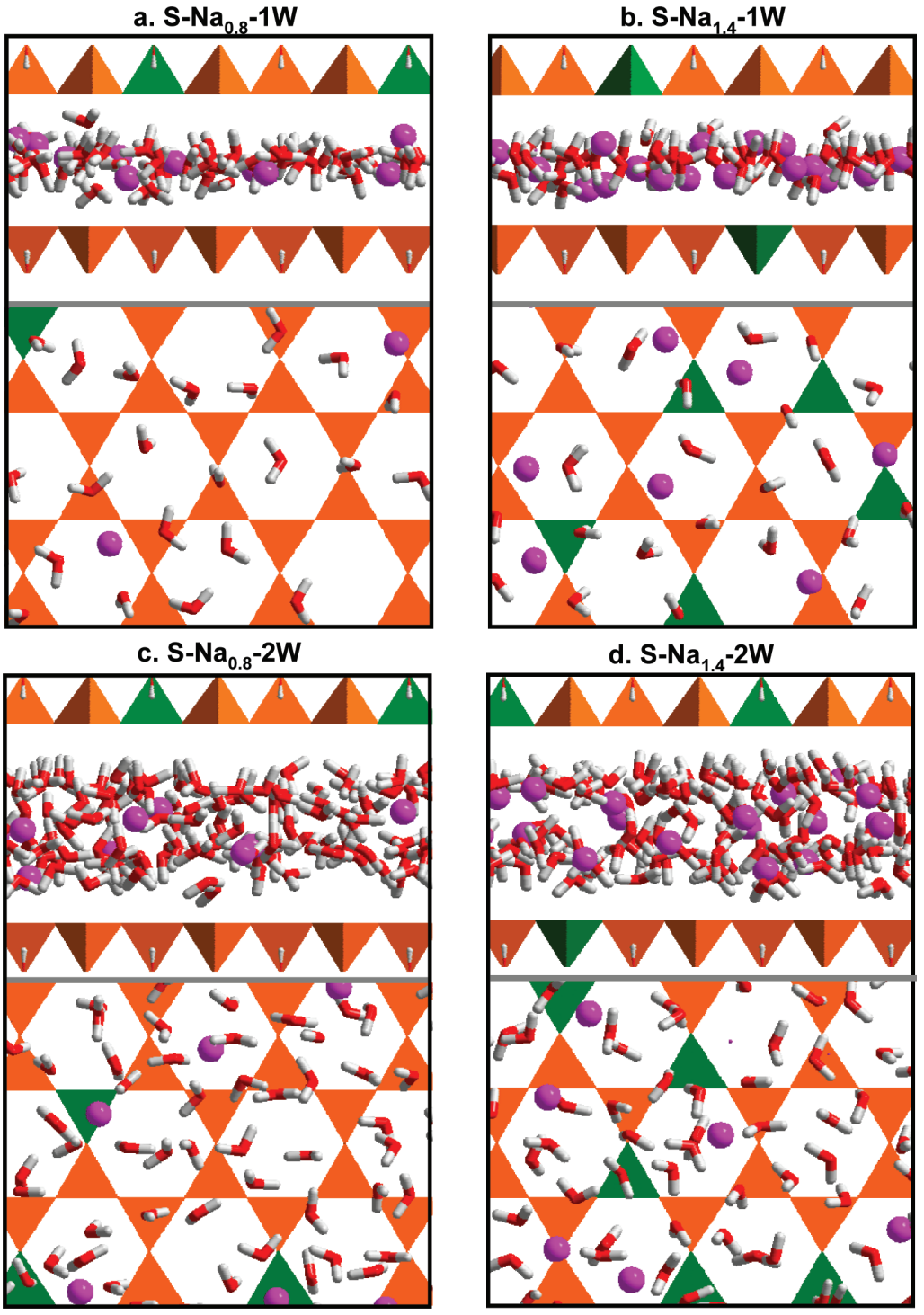

Figure 10. Snapshots of interlayer configuration (water molecules and sodium ions) calculated with the modified version of CLAYFF and SPC/E water models. (a) Monohydrated S−$Na_{0.8}$, (b) monohydrated S−$Na_{1.4}$, (c) bihydrated S−$Na_{0.8}$, and (d) bihydrated S−$Na_{1.4}$. Tetrahedral Si and Al are shown in orange and green, respectively. In the interlayer space, sodium, oxygen, and hydrogen atoms are shown in pink, red, and light gray, respectively. Each structure is displayed in projection both along the *b*- and the *c*-axes (top and bottom, respectively). A small portion of the simulation box is shown.

simplistic, and intrinsically biased, assessment of the clay and water model validity.

Structural Constraints. Despite its insensitivity toward hydrogen atoms (Figure 3), X-ray diffraction has proven its efficiency for assessing the computed interlayer electron density profiles, and the S/S-FF model was for example rejected on the sole basis of XRD. Similarly, the poor match between XRD patterns calculated for 2W saponites with the CLAYFF model and the data provided a first hint for modifying the LJ parameters of this model. Though not fully univocal, a proper fit of XRD patterns is thus an essential step in the validation of LJ parameters and atomic charges. However, neutron diffraction clearly represents

dx.doi.org/10.1021/jp105128r |*J. Phys. Chem. C* 2011, 115, 1867–1881

a step forward in the validation of clay and water models. Furthermore, using a short wavelength, as in the present study, allows increasing the constraints on the interlayer configuration model. On the other hand, using neutrons induces specific limitations. For example, the strong divergence of neutron beams significantly broadens 00*l* reflections,[69,70] thus leading to an apparent decrease of the CSD size [from about 12−16 layers for XRD to 5−7 for ND (Table 3)]. In addition, the combination of broad 00*l* reflections, large angular steps (0.125°2θ), and short wavelength (0.6966 Å) makes the calibration of experimental data difficult to perform and the detection of minor hydration heterogeneity almost impossible. The modification of ND reflection intensity distribution induced by the presence of minor hydration heterogeneity may lead to an erroneous assessment of interlayer models. A preliminary XRD characterization, such as that presented in the present series of papers,[10] is thus required to select the most appropriate experimental conditions, with minimum hydration heterogeneity. The combination of XRD and ND then provides a comprehensive data set owing to the scattering factor contrast between the two radiations (Figure 3). This combination is especially profitable for hydrated smectites when considering XRD and ND−D_2O data. Except for S−$Na_{1.4}$−2W, the interlayer profiles resulting from different clay and water models lead indeed to similar ND−H_2O diffraction patterns (Figures 6, 7, 8, and 9). This limited effect is related to the opposite signs of the coherent scattering length for oxygen (5.803 fm) and hydrogen (−3.739 fm). As a result, and because only periodicities ≥1.3 Å, which is, larger than the O−H distance in water (∼1 Å), were investigated, H_2O molecules can be considered as individual scatterers with negligible scattering length (−1.675 fm). In the experimental conditions used, H_2O molecules are thus "transparent" for neutrons, and ND−H_2O is essentially sensitive to the 2:1 layer structure. By contrast, water scattering dominates the calculated ND−D_2O profiles leading for example to the extinction of the 001 reflection for 1W saponite. This extinction, already observed for a similar saponite sample,[25] is extremely sensitive to the water content and orientation. The quality of sample deuteration is thus essential as incomplete H/D exchange would increase the 001 intensity, as observed on hydrogenated samples (Figures 6, 7, 8, and 9), and thus lead to an apparent lower water content. In this case, water sorption isotherms may provide key additional constraints to the structure model.

CONCLUSION AND PERSPECTIVES

When using well-characterized almost homogeneous synthetic clay samples, the combination of water adsorption measurements and X-ray and neutron diffraction provides an extensive data set that can be used for assessing thoroughly the validity of clay and water force fields. To be valid, a set of potentials must allow reproducing interlayer water contents, XRD, ND−H_2O, and ND−D_2O experiments for at least two layer charges and two hydration states. On the basis of these criteria, both the S/S-FF and the CLAYFF models show limitations, whereas a modification of the latter model (CLAYFF-Mod.) allowed reproducing the complete set of data. The proposed modification requires, however, further assessment before it can be generalized to other clay/water systems, especially by testing more recent and efficient clay models[56,58] when they are applicable to our samples. Additional collation of experimental and computational results for samples saturated with different cations and for samples with different layer charge location would be required, especially by considering a flexible clay model to fully assess the effect of the proposed modification on the structural feature of the clay layer. If validated, the proposed set of semiempirical potentials could be used to analyze the dynamical properties of interlayer water molecules and cations, taking into account the possible motion anisotropy. In a longer term perspective, any set of potentials who has passed the proposed validation could be used to analyze the structure and dynamics of water confined in the interlayer space of clay minerals.

AUTHOR INFORMATION

Corresponding Author

*Tel.: +33 (0)5 49 36 64 09. E-mail: eric.ferrage@univ-poitiers.fr.

ACKNOWLEDGMENT

Numerical simulations were performed at the "Centre de calcul en chimie quantique" (LACCO, Poitiers, France). The authors would like to thank Dr. Isabelle Bihannic and Camille Rivard (LEM, Nancy, France) for their help in the neutron diffraction experiments. EF gratefully acknowledges financial support from a European Marie-Curie Reintegration grant (Contract No. MERG-CT-2007-046413) and from a French ANR "Jeunes Chercheurs" program (Contract No. ANR-09-JCJC-0106-PorousClay). BS is grateful to the Russian Science Foundation and to the University of Poitiers for financial support during his stay in Poitiers. The authors would like to thank one of the two reviewers for his constructive comments that helped to improve the manuscript.

REFERENCES

(1) Burst, J. F. *Am. Assoc. Pet. Geol. Bull.* **1969,** *53*, 73.
(2) Freed, R. L.; Peacor, D. R. *Am. Assoc. Pet. Geol. Bull.* **1989,** *73*, 1223.
(3) Brown, K. M.; Ransom, B. *Geology* **1996,** *24*, 843.
(4) Boutareaud, S.; Calugaru, D. G.; Han, R.; Fabbri, O.; Mizoguchi, K.; Tsutsumi, A.; Shimamoto, T. *Geophys. Res. Lett.* **2008,** 35.
(5) Boullier, A. M.; Yeh, E. C.; Boutareaud, S.; Song, S. R.; Tsai, C. H. *Geochem., Geophys., Geosyst.* **2009,** *10*, 1.
(6) Matsuda, T.; Omura, K.; Ikeda, R.; Arai, T.; Kobayashi, K.; Shimada, K.; Tanaka, H.; Tomita, T.; Hirano, S. *Tectonophysics* **2004,** *378*, 143.
(7) Saffer, D. M.; Frye, K.; Marone, C.; Mair, K. *Geophys. Res. Lett.* **2001,** *28*, 2297.
(8) Vrolijk, P. *Geology* **1990,** *18*, 703–707.
(9) Michot, L. J.; Villieras, F.; Francois, M.; Bihannic, I.; Pelletier, M.; Cases, J. M. *C. R. Geosci.* **2002,** *334*, 611.
(10) Ferrage, E.; Lanson, B.; Michot, L. J.; Robert, J. L. *J. Phys. Chem. C* **2010,** *114*, 4515.
(11) Delville, A. *J. Phys. Chem.* **1993,** *97*, 9703.
(12) Chang, F. R. C.; Skipper, N. T.; Sposito, G. *Langmuir* **1995,** *11*, 2734.
(13) Chang, F. R. C.; Skipper, N. T.; Sposito, G. *Langmuir* **1997,** *13*, 2074.
(14) Marry, V.; Turq, P.; Cartailler, T.; Levesque, D. *J. Chem. Phys.* **2002,** *117*, 3454.
(15) Marry, V.; Turq, P. *J. Phys. Chem. B* **2003,** *107*, 1832.
(16) Boek, E. S.; Coveney, P. V.; Skipper, N. T. *J. Am. Chem. Soc.* **1995,** *117*, 12608.
(17) Boek, E. S.; Coveney, P. V.; Skipper, N. T. *Langmuir* **1995,** *11*, 4629.
(18) Smith, D. E. *Langmuir* **1998,** *14*, 5959.
(19) Shroll, R. M.; Smith, D. E. *J. Chem. Phys.* **1999,** *111*, 9025.
(20) Greathouse, J. A.; Storm, E. W. *Mol. Simul.* **2002,** *28*, 633.
(21) Skipper, N. T.; Sposito, G.; Chang, F. R. C. *Clays Clay Miner.* **1995,** *43*, 294.
(22) Skipper, N. T.; Refson, K.; McConnell, J. D. C. *J. Chem. Phys.* **1991,** *94*, 7434.

(23) Sposito, G.; Park, S. H.; Sutton, R. *Clays Clay Miner.* **1999,** *47,* 192.
(24) Young, D. A.; Smith, D. E. *J. Phys. Chem. B* **2000,** *104,* 9163.
(25) Rinnert, E.; Carteret, C.; Humbert, B.; Fragneto-Cusani, G.; Ramsay, J. D. F.; Delville, A.; Robert, J. L.; Bihannic, I.; Pelletier, M.; Michot, L. J. *J. Phys. Chem. B* **2005,** *109,* 23745.
(26) Ferrage, E.; Lanson, B.; Malikova, N.; Plançon, A.; Sakharov, B. A.; Drits, V. A. *Chem. Mater.* **2005,** *17,* 3499.
(27) Skipper, N. T.; Soper, A. K.; McConnell, J. D. C. *J. Chem. Phys.* **1991,** *94,* 5751.
(28) Sobolev, O.; Charlet, L.; Cuello, G.; Gehin, A.; Brendle, J. *Radiochim. Acta* **2008,** *96,* 679.
(29) Powell, D. H.; Tongkhao, K.; Kennedy, J. S.; Slade, P. G. *Clays Clay Miner.* **1997,** *45,* 290.
(30) Wexler, A. S. Constant humidity solutions. In *Handbook of Chemistry and Physics,* 74th ed.; Lide, D. R., Ed.; CRC press: Boca Raton, FL, 1994.
(31) Fischer, H. E.; Cuello, G. J.; Palleau, P.; Feltin, D.; Barnes, A. C.; Badyal, Y. S.; Simonson, J. M. *Appl. Phys. A-Mater. Sci. Process.* **2002,** *74,* S160.
(32) Sakharov, B. A.; Drits, V. A. *Clays Clay Miner.* **1973,** *21,* 15.
(33) Sakharov, B. A.; Lindgreen, H.; Salyn, A.; Drits, V. A. *Clays Clay Miner.* **1999,** *47,* 555.
(34) Drits, V. A.; Sakharov, B. A. *X-Ray structure analysis of mixed-layer minerals*; Doklady Akademii nauk SSSR: Moscow, 1976.
(35) Slade, P. G.; Stone, P. A.; Radoslovitch, E. W. *Clays Clay Miner.* **1985,** *33,* 51.
(36) Drits, V. A.; Sakharov, B. A.; Lindgreen, H.; Salyn, A. *Clay Miner.* **1997a,** *32,* 351.
(37) Allen, M. P.; Tildesley, D. J. *Computer Simulation of Liquids*; Oxford University Press: New York, 1994.
(38) Adams, D. J. *Mol. Phys.* **1975,** *29,* 307–311.
(39) Adams, D. J. *Mol. Phys.* **1974,** *28,* 1241–1252.
(40) Porion, P.; Faugère, A. M.; Delville, A. *J. Phys. Chem. C* **2008,** *112,* 11893.
(41) Porion, P.; Michot, L. J.; Faugère, A. M.; Delville, A. *J. Phys. Chem. C* **2007,** *111,* 5441.
(42) Michot, L. J.; Delville, A.; Humbert, B.; Plazanet, M.; Levitz, P. *J. Phys. Chem. C* **2007,** *111,* 9818.
(43) Pelletier, M.; Michot, L. J.; Humbert, B.; Barres, O.; D'espinose de la Callerie, J. B.; Robert, J. L. *Am. Mineral.* **2003,** *88,* 1801.
(44) Delville, A. *Langmuir* **1991,** *7,* 547.
(45) Karaborni, S.; Smit, B.; Heidug, W.; Urai, J.; Van Ort, E. *Science* **1996,** *271,* 1102.
(46) Chavez-Paez, M.; Van Workum, K.; de Pablo, L.; de Pablo, J. J. *J. Chem. Phys.* **2001,** *114,* 1405.
(47) Wang, J.; Kalinichev, A.; Kirkpatrick, R. J.; Hou, X. *Chem. Mater.* **2001,** *13,* 145.
(48) Meleshyn, A.; Bunnenberg, C. *J. Chem. Phys.* **2005,** *123,* 074706.
(49) Teppen, B. J.; Miller, D. M.; Newton, S. Q.; Schäfer, L. *J. Phys. Chem.* **1994,** *98,* 12545.
(50) Odriozola, G.; Aguilar, J. F.; Lopez-Lemus, J. *J. Chem. Phys.* **2004,** *121,* 4266.
(51) Zeng, Q. H.; Yu, A. B.; Lu, G. Q.; Standish, R. K. *J. Phys. Chem. B* **2004,** *108,* 10025.
(52) Newman, S. P.; Di Cristina, T.; Coveney, P. V.; W., J. *Langmuir* **2002,** *18,* 2933.
(53) Titiloye, J. O.; Skipper, N. T. *Mol. Phys.* **2001,** *99,* 899.
(54) Titiloye, J. O.; Skipper, N. T. *Chem. Phys. Lett.* **2000,** *329,* 23.
(55) Heinz, H.; Vaia, R. A.; Farmer, B. L. *J. Chem. Phys.* **2006,** *124,* 224713.
(56) Heinz, H.; Suter, U. W. *J. Phys. Chem. B* **2004,** *108,* 18341.
(57) Heinz, H.; Koerner, H.; Anderson, K. L.; Vaia, R. A.; Farmer, B. L. *Chem. Mater.* **2005,** *17,* 5658.
(58) Cygan, R. T.; Greathouse, J. A.; Heinz, H.; Kalinichev, A. G. *J. Mater. Chem.* **2009,** *19,* 2470.
(59) Cygan, R. T.; Liang, J. J.; Kalinichev, A. G. *J. Phys. Chem. B* **2004,** *108,* 1255.
(60) Whitley, H. D.; Smith, D. E. *J. Chem. Phys.* **2004,** *120,* 5387.
(61) Smith, D. E.; Wang, Y.; Chaturvedi, A.; Whitley, H. D. *J. Phys. Chem. B* **2006,** *110,* 20046.
(62) Skipper, N. T.; Chang, F. R. C.; Sposito, G. *Clays Clay Miner.* **1995,** *43,* 285.
(63) Berendsen, H. J. C.; Postma, J. P. M.; van Gunsteren, W. F.; Hermans, J. I. Interaction models for water in relation to protein hydration. In *Intermolecular Forces*; Pullman, B., Ed.; Reidel, D.: Amsterdam, 1981; p 331.
(64) Berendsen, H. J. C.; Grigera, J. R.; Straatsma, T. P. *J. Phys. Chem.* **1987,** *91,* 6269.
(65) Shroll, R. M.; Smith, D. E. *J. Chem. Phys.* **1999,** *110,* 8295.
(66) Heyes, D. M. *Phys. Rev. B* **1994,** *49,* 755.
(67) Hummer, G. *Chem. Phys. Lett.* **1995,** *235,* 297.
(68) Michot, L. J.; Bihannic, I.; Pelletier, M.; Rinnert, E.; Robert, J.-L. *Am. Mineral.* **2005,** *90,* 166.
(69) Ferrage, E.; Kirk, C. A.; Cressey, G.; Cuadros, J. *Am. Mineral.* **2007a,** *92,* 994.
(70) Ferrage, E.; Kirk, C. A.; Cressey, G.; Cuadros, J. *Am. Mineral.* **2007b,** *92,* 1007.